Performance of a virtual source model for stereotactic radiosurgery with a dynamic micro-multileaf collimator

W. González[1], M. Anguiano[2], A. M. Lallena[2]

[1]Laboratoire d'Imagerie et Modélisation en Neurobiologie et Cancérologie. CNRS-IN2P3. F-91405 ORSAY CEDEX. France.

[2]Departamento de Física Atómica, Molecular y Nuclear. Universidad de Granada. E-18071 Granada. Spain.

E-mail: wi12095@yahoo.es,mangui@ugr.es,lallena@ugr.es

Abstract. A virtual source model recently developed for external radiotherapy, which includes two photon sources and two electron sources, is tested for stereotactic radiosurgery with a dynamic micro-multileaf collimator. A 6 MV Elekta Precise linac that incorporates a 3Dline L'Arancio dynamic micro-multileaf collimator was considered. The capabilities of the virtual source model have been tested against full simulations performed with the Monte Carlo simulation code PENELOPE using both PENELOPE itself and the rapid Monte Carlo code DPM. The reference 10 cm × 10 cm radiation field as well as small fields of 1.2 cm × 1.2 cm, 2.9 cm × 2.9 cm and 5.8 cm × 5.8 cm were considered. The dynamic micro-multileaf collimator effect can be included in the virtual source model by reducing the width of the photon primary source by a factor 3. In all cases the virtual source model simulations were in very good agreement with the complete ones including the linac and collimator geometries.

1. Introduction

Monte Carlo (MC) simulation of linacs allows estimating in a rather accurate way the dose-to-patient with a particularly good description of situations such as those of interfaces in heterogeneous tissues, where other more conventional algorithms show inaccuracies difficult to be addressed (Chetty *et al* 2007). Among other approaches, virtual source models (VSMs) have been extensively considered in commercial MC dose calculation engines now available: eMC in Eclipse (Fix *et al* 2013), the VSM of Fippel *et al* (2003) incorporated in iPlan RT Dose, the VSM of Sikora *et al* (2007) and Sikora and Alber (2009) used in Monaco, the multi-source model of Traneus *et al* (2001) implemented in Oncentra, or the VSM of XiO (Vandervoort *et al* 2014). These models are based on a set of analytical particle sources that describe the radiation reaching the patient and that can be tuned according to the information obtained from each particular linac considered (Fippel *et al* 2003, Yang *et al* 2004, Sikora *et al* 2007, González *et al* 2015a, 2015b). The beams emitted from these sources are transported

using a MC code for calculating doses in a given target (a water phantom for physical dosimetry or a patient phantom in case of clinical dosimetry or treatment planning verification).

Recently, a general VSM for clinical linac heads in photon mode including two photon and two electron sources has been developed (González *et al* 2015a, 2015b). The photon sources describe the primary and scatter photon fluences while the electron sources take care of the electron contamination produced in the linac head and in the air between the linac and the target. The model was tested for 3 linacs: an Elekta Precise (Elekta Group, Crawly, UK), with qualities of 6 and 15 MV, and a Varian Clinac 2300C/D (Varian Medical System, Palo Alto, CA) and a Siemens Mevatron KDS (Siemens Medical Systems, Oncology Care Systems, Concord, USA), both with qualities 6 and 18 MV. In all cases a good description of the linac radiation entering patients, including both photons and electrons, was achieved. For photons (González *et al* 2015b) the overall agreement was estimated on the base of a gamma test for PDDs and both in- and off-axis transverse profiles. The results were compared to those provided by the commonly used VSM model of Fippel *et al* (2003). Except in a few cases, the results obtained with our VSM were much better. For electrons (González *et al* 2015a), it was shown that the presence of the second electron source is mandatory to have a correct description of the electron PDDs and transverse profiles. To do that we compared the results obtained with our VSM to those found with the model of Sikora and Alber (2009) that includes an electron source only.

Stereotactic radiosurgery (SRS), as a minimally invasive surgical technique, has shown a noticeable impact on the treatment of patients with cerebral neoplasias, vascular malformations, focal epileptic lesions and other functional and behavioral disorders. Treatments are delivered with Gamma Knife®, CyberKnife and also with linacs. In this last case the emerging beam is collimated with either a micro-multileaf collimator or a set of cone collimators. These collimators produce the small radiation fields needed, with apertures of a few millimeters at the isocenter, what requires a very good geometric and dosimetric accuracy.

These dose measurements for these small radiation fields are strongly demanding because the detector sizes are, in some cases, similar to field sizes, a loss of lateral charged particle equilibrium occurs, the source is partially occluded and there are non-negligible dependences on the beam energy, the focal spot size, the detector positioning or the jaw geometry (Paskalev *et al* 2003, Sham *et al* 2008, Scott *et al* 2008). Dosimetry uncertainties for SRS small fields may be considerably large (Das *et al* 2008) and the discrepancies with MC calculations can be significant and depend on the detector used in the measurements (Alfonso *et al* 2008). All these characteristics make SRS with a linac an exigent situation to test the actual capabilities of MC simulations with a VSM.

The purpose of the present work was to address the performance of the VSM of González *et al* (2015a, 2015b) for SRS carried out with a linac supplemented with a dynamic micro-multileaf collimator (DMLC). Specifically, a 6 MV Elekta Precise linac that incorporates a dynamic micro-multileaf collimator (DMLC) model 3Dline L'Arancio

(3D Line Research and Development, Elekta Group, Crawley, UK) was studied. The way how to incorporate the DMLC in the VSM in order to analyze its capabilities for SRS treatment plan verification was analyzed.

2. Material and methods

The VSM used in the present work is that developed by González *et al* (2015a, 2015b). It consists of four sources. Two of them are the primary and scatter photon sources. The other two take care of the electron contamination: one of them describes the electrons produced in the linac head and the other corresponds to the electrons produced in the air between the linac head and the patient. The specific details for the 6 MV Elekta Precise linac that is considered in the present work are given in appendix A.

In order to perform simulations with the VSM, it was necessary to establish the relative weight of photon and electron sources. In our case this was done by analyzing the contents of a phase-space file scored at the phantom surface for a $10\,\text{cm} \times 10\,\text{cm}$ field. Specifically we considered 99.45% for photons and 0.52% for electrons. The remaining 0.03% was due to positrons that were not considered in the present calculations.

To test the VSM, the results of the different simulations performed with that model were compared to those found in simulations carried out with the complete geometry of the linac. As described in appendix B, these latter simulations were benchmarked against experimental measurements in a previous work (González *et al* 2011). In the cases where the DMLC was included, we followed the procedure described in appendix B. These simulations were done with the version 2014 of the MC code PENELOPE (Salvat *et al* 2014). The code permits to simulate the coupled transport of photons, electrons and positrons in any material and geometry. All details about the code and the tracking parameters can be found in the PENELOPE user manual (Salvat *et al* 2014).

In addition to the simulations performed with PENELOPE, a set of simulations were carried out with DPM (Sempau *et al* 2000), using the VSM and a simplified geometry of the DMLC. In these simulations the DMLC was assumed to be a simple aperture (the actual one of the DMLC in each radiation field) collimating mathematically the corresponding beams generated at the sources, without additional details. With these simulations the capabilities of the VSM in actual applications were further analyzed.

In all these simulations, doses were calculated in a water phantom of $30\,\text{cm} \times 30\,\text{cm} \times 40\,\text{cm}$, with a source-to-surface distance of 100 cm. Scoring voxels of $0.10\,\text{cm} \times 0.20\,\text{cm} \times 0.35\,\text{cm}$ were considered.

3. Results and discussion

In the previous works by González *et al* (2015a, 2015b) the electron and photon components of the VSM were analyzed independently. Then the first comparison to

be done must check the capability of the whole VSM. To do that we compared the complete MC simulation, including the detailed geometry of the linac head, and that performed with the VSM for the 6MV Elekta Precise linac in reference conditions, with a radiation field of 10 cm × 10 cm at the surface of the water phantom and a source-to-surface distance of 100 cm. The results obtained are shown in figure 1.

Panel (a) shows that the PDDs obtained in both calculations are in good agreement, with relative differences (see dotted curve) below 2%, except in the phantom surface (at $z \sim 0$). The transverse profiles obtained with the VSM (solid and dashed curves in panel (b)) are also in good agreement with those provided by the complete MC simulation

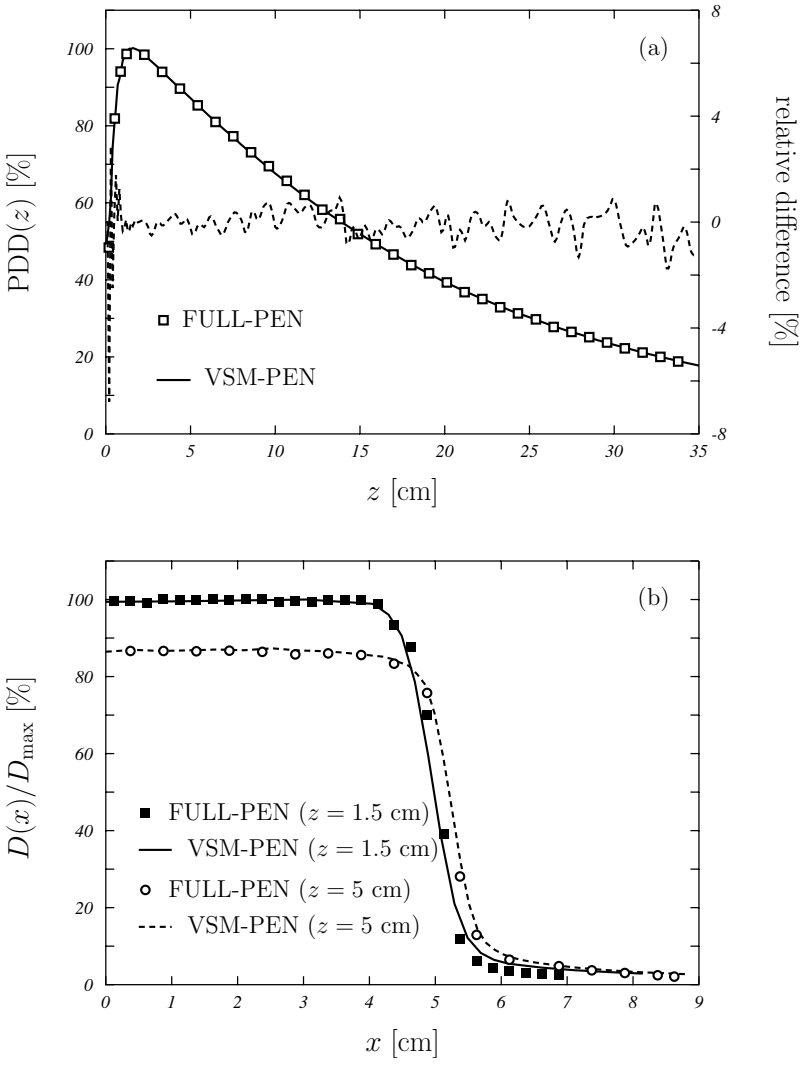

Figure 1. Comparison of (a) the PDD and (b) two profiles at depths of 1.5 and 5 cm obtained with the VSM (curves) with those found in the complete MC simulation including the detailed linac geometry (symbols), both with PENELOPE. A radiation field of 10 cm× 10 cm at the phantom surface and a source-to-surface distance of 100 cm was considered. Uncertainties are show with a coverage factor $k = 3$. The dashed curve in panel (a) represents the relative difference between both calculations and is referred to the right ordinate axis.

(symbols) at the two depths considered. Up to $x \sim 4.5\,\mathrm{cm}$, the differences between both calculations are smaller than 1.5%. In the penumbrae these differences are below 5%, with a distance to agreement smaller than 1 mm. In particular, the maximum discrepancy at the depth of the maximum dose ($z = 1.5\,\mathrm{cm}$) is $\sim 1\,\mathrm{mm}$ and appears at the penumbra. In any case all differences are within the limits established by the IAEA (2004).

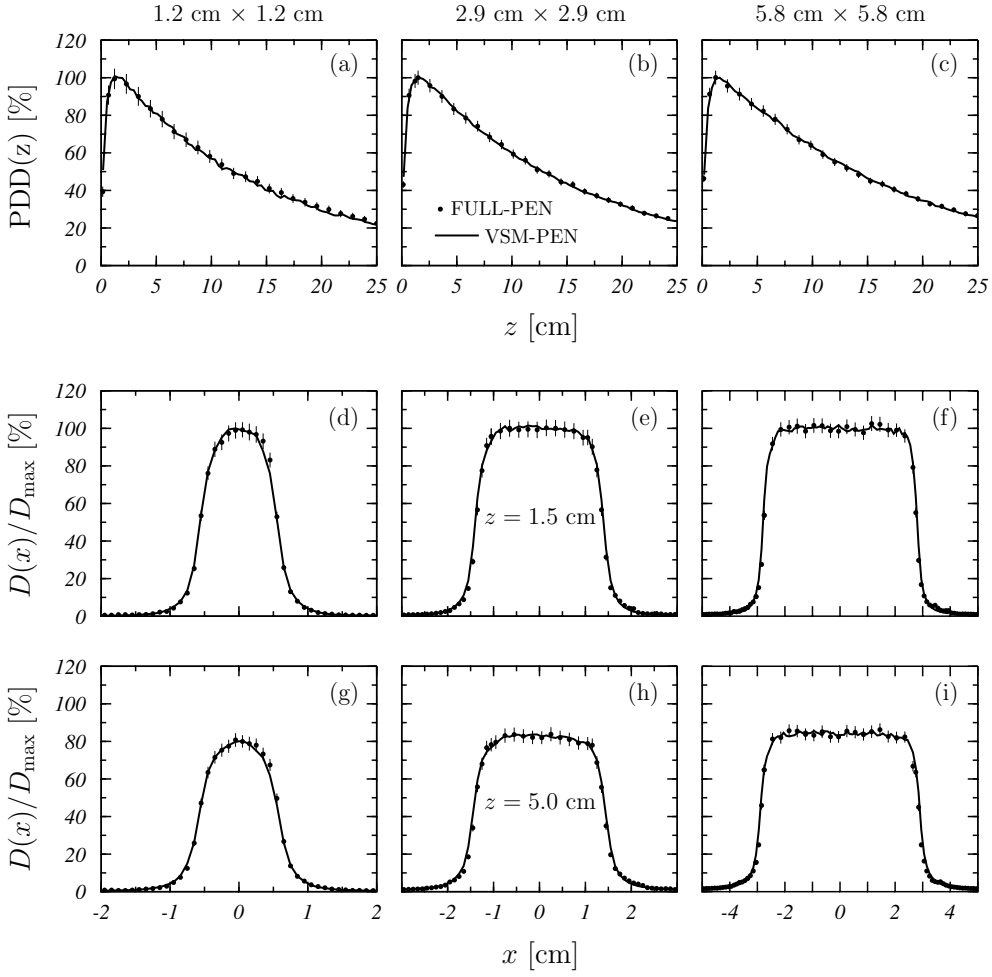

Figure 2. PDDs (panels (a)-(c)) and normalized transverse profiles at depths $z = 1.5\,\mathrm{cm}$ (panels (d)-(f)) and $z = 5\,\mathrm{cm}$ (panels (g)-(h)) for radiation fields of $1.2\,\mathrm{cm} \times 1.2\,\mathrm{cm}$, $2.9\,\mathrm{cm} \times 2.9\,\mathrm{cm}$, $5.8\,\mathrm{cm} \times 5.8\,\mathrm{cm}$. Solid curves represent the results obtained with the VSM and solid circles those found with the complete MC simulation including the DMLC. These calculations were performed with PENELOPE. Uncertainties are given with a coverage factor $k = 2$.

In figure 2, the results obtained with the complete MC simulation including the DMLC are compared to those found with the VSM. Panels (a)-(c) show the PDDs; the normalized transverse profiles at depths $z = 1.5$ and 5 cm are shown in panels (d)-(f) and (g)-(i), respectively. The VSM reproduces very well both the PDDs and the transverse profiles obtained with the complete MC simulation. The relative differences around the maximum of the PDDs corresponding to the three radiation fields, as well as in the

maximum region of the transverse profiles, were 2% at most. In the penumbrae the distance to agreement between the profiles obtained by using VSM and the reference ones were smaller than 0.5 mm. This opens the possibility of using the VSM as a tool for verification of treatment plans in SRS.

In order to complete the analysis of the feasibility of the VSM, DPM simulations were done in which the DMLC was considered as a simple aperture producing a mathematical collimation of the beams. The aim was addressing the modifications required to incorporate the DMLC collimation effects in the VSM.

Figure 3 shows the results of the DPM simulation (dashed curves) in comparison with the results of the complete MC simulation performed with PENELOPE. Some non-negligible discrepancies appear and the profiles obtained with DPM+VSM are

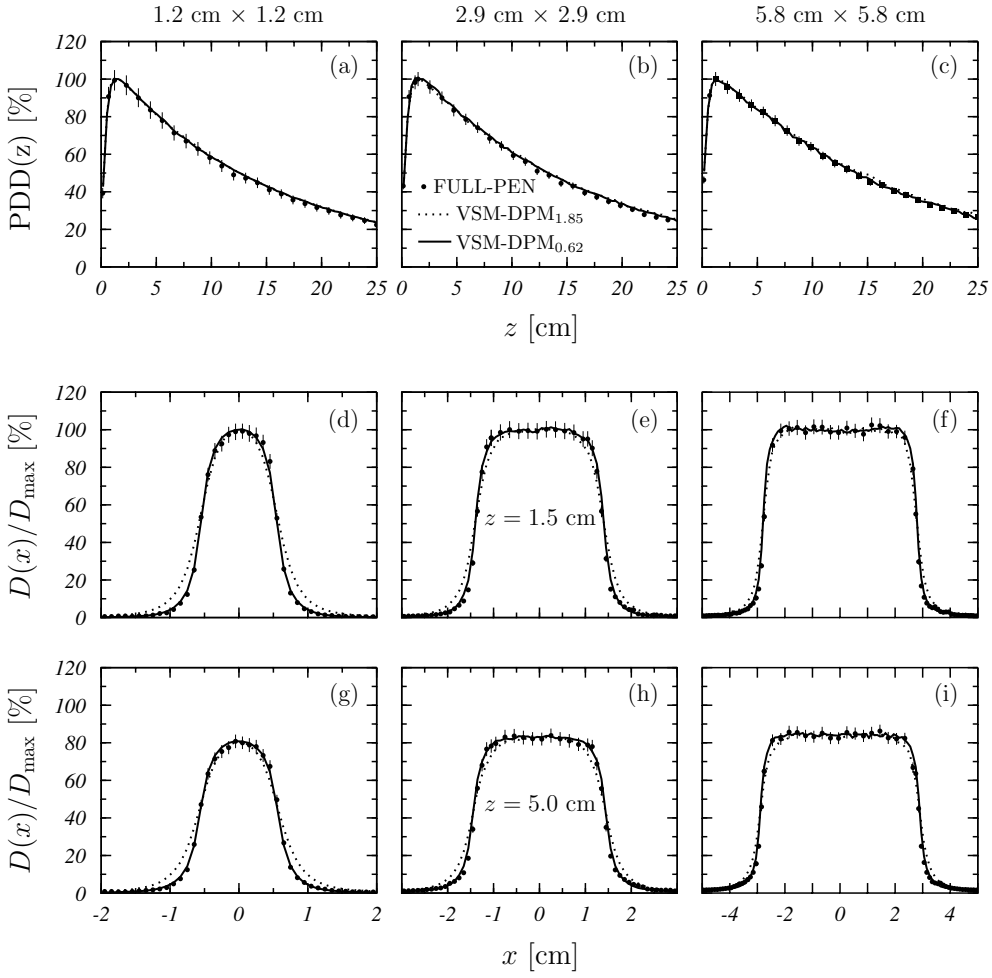

Figure 3. Same as in figure 2 but comparing the results of the complete PENELOPE MC simulation including the DMLC (solid circles) with those obtained with DPM+VSM and the simplified geometry of the DMLC. In this last case, calculations performed with two different values of the parameter δ_0 defining the width of the photon primary source are shown: dotted curves correspond to $\delta_0 = 1.85\,\text{cm}$ and solid curves to $\delta_0 = 0.62\,\text{cm}$. Uncertainties correspond to a coverage factor $k = 2$.

Table 1. Values of the penumbrae, in cm, for the profiles of figure 3. Results for the three field sizes considered and the two depths in water are shown. Uncertainties with a coverage factor $k = 2$ are 0.1 mm in all cases.

	PENELOPE (complete geometry)		DPM+VSM			
			$\delta_0 = 1.85$		$\delta_0 = 0.62$	
field size	$z = 1.5$ cm	$z = 5$ cm	$z = 1.5$ cm	$z = 5$ cm	$z = 1.5$ cm	$z = 5$ cm
1.2 cm × 1.2 cm	0.27	0.28	0.43	0.45	0.28	0.28
2.9 cm × 2.9 cm	0.27	0.30	0.45	0.52	0.29	0.30
5.8 cm × 5.8 cm	0.30	0.30	0.50	0.51	0.29	0.29

wider than the PENELOPE ones. As a consequence, the corresponding penumbrae are larger, as can be seen in table 1: the values obtained for DPM+VSM are systematically $\sim$ 2 mm larger than those obtained in the PENELOPE reference calculation. This could be expected because in the definition of the limits $x_\alpha^\pm$ and $y_\alpha^\pm$ of the regions of the sources that are effectively seen from the calculation points, the DMLC was not included. However, the presence of the DMLC modifies these limits producing, in general, a reduction of the source region viewed.

In other words, there is a reduction of the width of the sources. The solid curves in figure 3 have been obtained also with DPM but by reducing the parameter δ_0 from the original value of 1.85 cm to 0.62 cm. The new profiles agree nicely with those of the complete PENELOPE MC simulation. This can be also seen in table 1: the penumbrae values obtained for DPM+VSM with $\delta_0 = 0.62$ coincide with the reference ones within uncertainties.

A proper consideration of the DMLC in the VSM would require a fitting of the model fluences (see the appendix) to in-air fluence profiles below the collimator, with the modifications that eventually could introduce its different configurations. However, the results shown in figure 3 indicate that the global effect of the DMLC may be taken into account by reducing the size of the photon primary source, independently of its aperture. In addition, these results point out the consistency and flexibility of our VSM to account for relevant changes in the collimation system used.

To finish we would like pointing out that the computing time is strongly reduced in the DPM+VMS calculations with respect to the reference ones, performed with PENELOPE and considering the complete geometry. The reduction ratios are $\sim$ 40 for the two smaller field sizes and $\sim$ 20 for the 5.8 cm × 5.8 cm field. In these values the computing time required to score the PSFs needed in the complete reference simulation (see appendix B) are not included.

4. Conclusions

In this work a VSM recently developed for describing the dose delivered by radiotherapy treatment linacs has been tested in SRS with a DMLC. The VSM, that had been fitted

using radiation fields with dimensions of the order of 10 cm, is able to reproduce the results obtained with a complete MC simulation including the detailed geometry of the DMLC, for small fields of up to 5.8 cm × 5.8 cm.

A simulation performed with DPM, considering that the DMLC is described in terms of a simple mathematical collimation of the beams generated in the various sources of the VSM, produced transverse profiles with widths larger than those obtained with the detailed PENELOPE simulation. This meant that the presence of the DMLC cannot be simulated in such a simple way because it modifies the characteristics of the sources and, in particular, the area of them that is seen from the calculation point. It has been shown that by reducing by a factor ~ 3 the width of the photon primary source a good agreement is found between the simplified DPM and the detailed and complete PENELOPE simulations.

The results found in this work point out the consistency of the VSM studied and its flexibility to incorporate strong modifications in the collimation system.

Acknowledgements

This work has been partially supported by the Spanish Ministerio de Economía y Competitividad (FPA2015-67694-P), European Regional Development Fund (ERDF) and by the Junta de Andalucía (FQM0387). Authors acknowledge the CPU time granted at Calendula Castilla y León Supercomputing Center and Mare Nostrum Barcelona Supercomputing Center (National RES access program, Spanish Supercomputing Network Area).

Appendix A. Virtual source model for the 6MV Elekta Precise linac

The VSM used for the 6 MV Elekta linac considered in the present work was that developed by González *et al* (2015a, 2015b). It consisted of four sources that describe the primary and scattered photons and the electron contamination. The situation of these four sources is shown in the scheme of figure 4.

The photon fluence at the point (x, y, z) was assumed to be of the form (González *et al* 2015b):

$$\phi_\gamma(x,y,z) \,=\, w_0\,\phi_0(x,y,z)\,\phi^\gamma_{\rm horn}(x,y,z) \,+\, (1\,-\,w_0)\,\phi_{\rm s}(x,y,z)\,. \qquad (1)$$

The functions ϕ_0 and $\phi_{\rm s}$ represent the fluences produced by the primary and scatter sources. The primary source was situated at the point $(x_0, y_0, z_0) = (0, 0, 0)$, that is, 100 cm upstream the isocenter, which is at $(x_{\rm I}, y_{\rm I}, z_{\rm I}) = (0, 0, 100\,{\rm cm})$, just on the entrance surface of the target. The position of the scatter source, at $(x_{\rm s}, y_{\rm s}, z_{\rm s}) = (0, 0, 15.8\,{\rm cm})$, was just below the flattening filter of the linac.

On the other hand, the VSM model assumes that the total fluence due to electrons at a point (x, y, z) is of the form (González *et al* 2015a):

$$\phi_{\rm e}(x,y,z) \,=\, w_{\rm h}\,\phi_{\rm h}(x,y,z)\,\phi^{\rm e}_{\rm horn}(x,y,z) \,+\, (1\,-\,w_{\rm h})\,\phi_{\rm a}(x,y,z)\,, \qquad (2)$$

where $\phi_{\rm h}(x,y,z)$ is the fluence due to the electrons produced in the linac head and $\phi_{\rm a}(x,y,z)$ is that corresponding to the electrons produced in-air. The first electron source was at the same point than the photon scatter source, while that corresponding to the in-air electron contamination produced was situated at $(x_{\rm a}, y_{\rm a}, z_{\rm a}) = (0, 0, 29.8\,{\rm cm})$, that is just above the secondary collimation system of the linac.

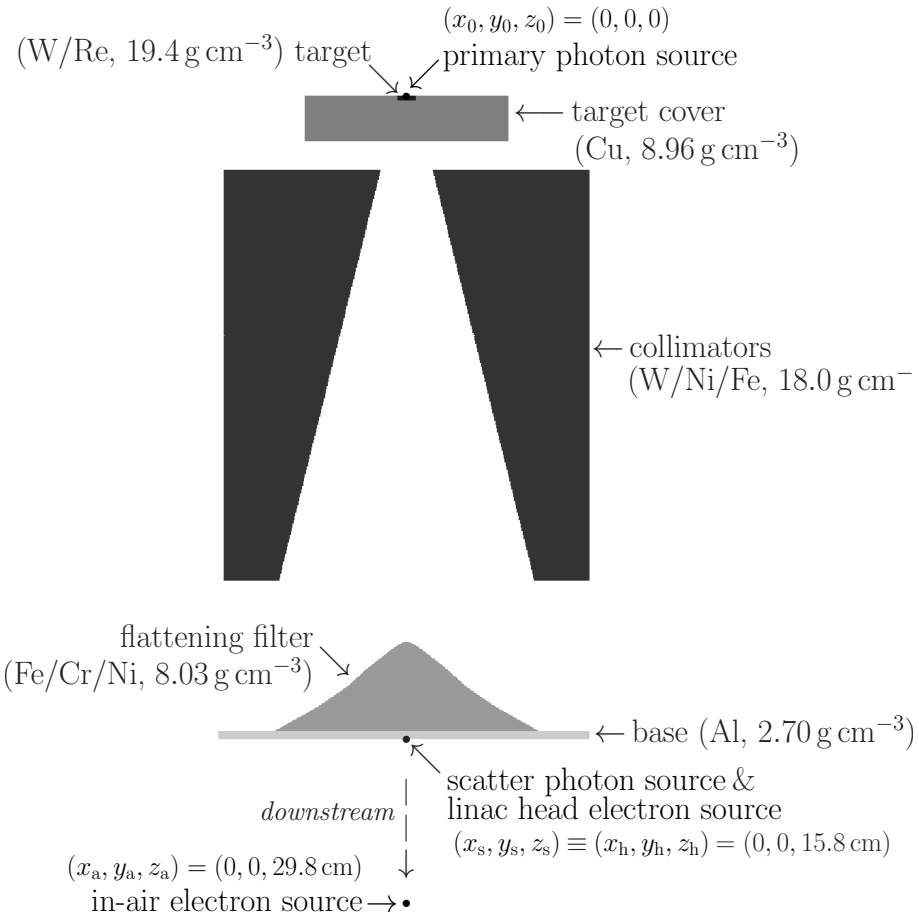

Figure 4. Scheme of the head of the 6 MV Elekta Precise linac considered in the present work. The position of the four sources included in the VSM are indicated. The primary photon source was situated at the target entrance surface; the scatter photon and linac head electron sources were at the output surface of the base of the flattening filter, and the in-air electron contamination source is situated downstream, just below the secondary collimation system of the linac. The target, primary collimator and flattening filter are shown including the elements or alloys of which they are built up and their densities.

All the spatial fluence distributions are of the form:

$$\phi_\alpha(x,y,z) \;=\; \mathcal{Z}(z; z^x_{\rm D}, z^y_{\rm D}, z_\alpha)\, \mathcal{T}_\alpha(x^+_\alpha, x^-_\alpha)\, \mathcal{T}_\alpha(y^+_\alpha, y^-_\alpha)\,, \tag{3}$$

with

$$\mathcal{Z}(z; z^x_{\rm D}, z^y_{\rm D}, z_\alpha) \;=\; \frac{1}{4}\,\frac{(z^x_{\rm D} - z_\alpha)(z^y_{\rm D} - z_\alpha)}{(z - z_\alpha)^2}\,, \tag{4}$$

which is related to the reduction of the fluence with the inverse of the square of the distance to the source,

$$\mathcal{T}_0(t_0^+, t_0^-) \,=\, Q_0\left(\frac{t_0^+}{\delta_0}\right) \,+\, Q_0\left(\frac{t_0^-}{\delta_0}\right)\,, \tag{5}$$

for the photon primary source, with $Q_0(v) = v/\sqrt{1+v^2}$, and

$$\mathcal{T}_\alpha(t_\alpha^+, t_\alpha^-) \,=\, \mathrm{erf}\left(\frac{t_\alpha^+}{\sqrt{2}\sigma_\alpha}\right) \,+\, \mathrm{erf}\left(\frac{t_\alpha^-}{\sqrt{2}\sigma_\alpha}\right)\,, \tag{6}$$

for the photon scatter ($\alpha = \mathrm{s}$) and the two electron ($\alpha = \mathrm{h}, \mathrm{a}$) sources. Here erf labels the well known error function. In the two previous equations t stands for x or y.

The values $x_\alpha^\pm$ and $y_\alpha^\pm$ are the extremes delimiting the region of the source seen from the calculation point (x, y, z); they are given by

$$x_\alpha^\pm \,=\, \min\left[\frac{w_\mathrm{I}^x\, z_\mathrm{U}^x\,(z - z_\alpha) \pm 2\,x\, z_\mathrm{I}\,(z_\alpha - z_\mathrm{U}^x)}{2 z_\mathrm{I}\,(z - z_\mathrm{U}^x)}, \frac{w_\mathrm{I}^x\, z_\mathrm{D}^x\,(z - z_\alpha) \pm 2\,x\, z_\mathrm{I}\,(z_\alpha - z_\mathrm{D}^x)}{2 z_\mathrm{I}\,(z - z_\mathrm{D}^x)}\right] \tag{7}$$

and

$$y_\alpha^\pm \,=\, \min\left[\frac{w_\mathrm{I}^y\, z_\mathrm{U}^y\,(z - z_\alpha) \pm 2\,y\, z_\mathrm{I}\,(z_\alpha - z_\mathrm{U}^y)}{2 z_\mathrm{I}\,(z - z_\mathrm{U}^y)}, \frac{w_\mathrm{I}^y\, z_\mathrm{D}^y\,(z - z_\alpha) \pm 2\,y\, z_\mathrm{I}\,(z_\alpha - z_\mathrm{D}^y)}{2 z_\mathrm{I}\,(z - z_\mathrm{D}^y)}\right]\,. \tag{8}$$

Here $z_\mathrm{U}^x = 43.1\,\mathrm{cm}$, $z_\mathrm{U}^y = 29.8\,\mathrm{cm}$, $z_\mathrm{D}^x = 50.9\,\mathrm{cm}$ and $z_\mathrm{D}^y = 42.6\,\mathrm{cm}$ are the upstream and downstream z-coordinates of the collimation system in the directions x and y. The DMLC is treated separately (see text and Appendix B) and is not included is these values. Finally, w_I^x and w_I^y indicate the field size at the isocenter in the directions x and y, respectively.

The function $\phi_\mathrm{horn}^\gamma$ was included in the definition of the photon primary source in equation (1) to take into account the effect of the flattening filter, which produces the central depression shown by the fluence profiles. In the case of the electron fluence (see equation (2)), the function $\phi_\mathrm{horn}^\mathrm{e}$ was introduced, for analogy with the photon fluence, to describe possible variations between the central part of the electron radiation fields and their edges, permitting an easier fit of the VSM to actual electron transverse profiles. In the VSM these two functions were assumed to be of the form

$$\phi_\mathrm{horn}^{\gamma,\mathrm{e}}(x, y, z) \,\equiv\, \phi_\mathrm{horn}^{\gamma,\mathrm{e}}(\rho) \,=\, 1 \,+\, \rho^2 \sum_{j=0}^{4} h_j^{\gamma,\mathrm{e}}\, \rho^j\,, \tag{9}$$

with $\rho = \sqrt{x^2 + y^2}/(z - z_0)$.

In the case of photons, the VSM includes various fitting parameters: w_0, the relative weight of the photon primary source (see equation (1)), δ_0 and σ_s, which are related to the spatial width of the primary and scatter sources, respectively (see equations (5) and (6)) and the h_j^γ parameters of the $\phi_\mathrm{horn}^\gamma$ function defined in equation (9). To determine their values the photon fluence model in equation (1) was fitted to a series of in-air photon fluence profiles obtained in MC simulations performed with the complete linac geometry. These profiles corresponded to field sizes of 2×2, 3×3, 5×5, 10×10, 20×20, 40×40, 5×40, 10×40, 40×5, 40×10 and $40\times40\,\mathrm{cm}^2$. For each one of them the profile in the beam direction ($x = y = 0$) for z between 85 and 115 cm, three profiles in the x

direction ($y = 0$) and three additional ones in the y direction ($x = 0$), for $z = 85$, 100 and 115 cm were included in the fitting procedure. The values obtained for the fitting parameters are those given in table 2.

Table 2. Values of the fitting parameters of the photon and electron sources for the 6 MV Elekta Precise linac. Photon parameters are from González *et al* (2015b) and those of electrons from González *et al* (2015a). Uncertainties with a coverage factor $k = 1$ are given between parentheses; that is, 24.7(1.5) means 24.7 ± 1.5.

photons		electrons	
w_0	0.958(1)	w_h	0.100(6)
δ_0	1.85(2) mm	σ_h	16.6(6) mm
σ_s	24.7(1.5) mm	σ_a	33.9(5) mm
h_0^γ	151.3(4.6)	h_0^e	111.6(3.3)
h_1^γ	-4505.9(153.1)	h_1^e	3.48(7)
h_2^γ	55383.5(1875.0)	h_2^e	488.4(39.1)
h_3^γ	-295681.0(9825.0)	h_3^e	-2973.0(178.3)
h_4^γ	571317.0(18630.0)	h_4^e	-683.3(61.1)

In the case of the electron sources, the fitting parameters are the relative weight of the head electron source, w_h (see equation (2)), the estimations of the spatial width of the two electron sources, σ_h and σ_a (see equation (6)), and the h_j^e parameters defining the $\phi_\mathrm{horn}^\mathrm{e}$ function (see equation (9)). Similarly to what was done for the photon fluence, the electron fluence model in equation (2) was fitted to the corresponding in-air electron fluence profiles obtained in the complete MC simulations mentioned above. This permitted to obtain the values given in table 2.

In what refers to energy distributions, it is assumed that photons coming from the primary source and moving in the beam axis show a spectrum of the form (González *et al* 2015b):

$$p_0(E) \;=\; N_0 \,\frac{\mathcal{E}(E; b_0, E_\mathrm{max}^\gamma) \;-\; 1}{\mathcal{E}(0; b_0, E_\mathrm{max}^\gamma)} \,\left[1 \;-\; \mathcal{E}(E; s_0, E_\mathrm{min}^\gamma)\right] \,, \tag{10}$$

where

$$\mathcal{E}(E; \kappa, \epsilon) \;=\; \exp\left[\kappa\,(\epsilon - E)\right] \,. \tag{11}$$

This function was fitted to the distribution of photons coming from the primary source, moving along the beam axis and reaching the plane just below the flattening filter, obtained in the MC simulation performed with the complete geometry of the linac. On the other hand, the energies E_max^γ and E_min^γ are the maximum and minimum energies scored for these photons. The values obtained for the parameters are given in table 3.

The energy spectra of the photons emitted from the primary source and moving in a direction other than the beam axis was

$$p_0(E, \theta) \;=\; \epsilon(\theta)\, p_0(E) \,, \tag{12}$$

where θ is the polar angle (in degrees) of the emission direction of the photon,

$$\epsilon(\theta) \,=\, \left[1 \,+\, 0.00181\,\theta \,+\, 0.00202\,\theta^2 \,-\, 0.0000942\,\theta^3\right]^{-1/\nu} \,, \tag{13}$$

and ν is a free parameter that is determined by fitting the average energy corresponding to each polar angle to the corresponding one obtained in the complete MC simulation.

Finally, for the photons emitted from the scatter source, the energy was taken to be

$$E_{\mathrm{S}} \,=\, E\,\left[1 \,+\, (1-\cos\beta)\,\frac{E}{m_e c^2}\right]^{-1} \,, \tag{14}$$

where β is the angle between the directions of the previous primary photon, which had an energy E, and the scatter one, and m_e is the electron rest mass.

In what refers to the spectrum energy of electrons emitted from the head and in-air sources, the VSM considered the same distribution (González *et al* 2015a):

$$p_{\mathrm{e}}(E) \,=\, N_{\mathrm{e}}\,\frac{\mathcal{E}(E;b_{\mathrm{e}},E^{\mathrm{e}}_{\mathrm{max}}) \,-\, 1}{\mathcal{E}(0;b_{\mathrm{e}},E^{\mathrm{e}}_{\mathrm{max}})}\,\left[1 \,-\, \mathcal{E}(E;s_{\mathrm{e}},E^{\mathrm{e}}_{\mathrm{min}})\right] \,. \tag{15}$$

The free parameters where determined by fitting this distribution to the energy spectrum of the electrons reaching the phantom surface obtained in the complete MC simulation. On the other hand, the energies $E^{\mathrm{e}}_{\mathrm{max}}$ and $E^{\mathrm{e}}_{\mathrm{min}}$ are the maximum and minimum energies scored for these electrons. The values of these parameters are given in table 3.

All fitting procedures were carried out using the Levenberg-Marquardt minimization method (Press *et al* 1992).

Appendix B. Details of the simulations of the linac and DMLC

As indicated above, some of the simulations carried out with PENELOPE included the complete geometry of the 6 MV Elekta Precise linac and that of the DMLC. The linac geometry was built up according to some information provided by the manufacturer. Figure 4 shows some details of the linac head, in particular the target, the primary collimator and the flattening filter.

A monoenergetic electron beam with an initial energy of 6.3 MeV and a spatial distribution of Gaussian type, with a full width at half-maximum of 1.2 mm impinges on the target producing the photon beam.

Table 3. Values of the parameters of the energy distributions p_0, as defined in equation (10), the parameter ν introduced in equation (13), and the parameters of the distribution p_{e}, as given in equation (15).

	N_0 (MeV^{-1})	b_0 (MeV^{-1})	s_0 (MeV)$^{-1}$	$E^{\gamma}_{\mathrm{min}}$ (MeV)	$E^{\gamma}_{\mathrm{max}}$ (MeV)	ν
photons	0.10(2)	0.46(4)	4.68(6)	0.15	6.3	0.4
	N_{e} (MeV^{-1})	b_{e} (MeV^{-1})	s_{e} (MeV)$^{-1}$	$E^{\mathrm{e}}_{\mathrm{min}}$ (MeV)	$E^{\mathrm{e}}_{\mathrm{max}}$ (MeV)	
electrons	0.08(1)	0.60(1)	24.9(4)	0.10	6.0	

The materials conforming the head are also given in figure 4. The target is made of an alloy of W/Re and is embedded in a Cu block. The primary collimator is made of W/Ni/Fe. A flattening filter made of Fe/Cr/Ni is included.

The radiation fields were conformed with a collimation system consisting of a pair of upper jaws in the y-direction and a pair of lower jaws in the x-direction. In addition, this linac incorporated a multileaf collimator situated just above the upper jaws. In our simulations it has been considered together with the y-pair of jaws (see González et al., 2011 for details.)

Simulations were performed with the version 2014 of PENELOPE (Salvat et al., 2014). The values of the simulation parameters used in our simulations for each material in the geometry are those given in table 4.

Table 4. Values of the simulation parameters used in our simulations for the various materials in the linac geometry.

Material	C1	C2	WCC (keV)	WCR (keV)	EABS(γ) (keV)	EABS(e^-) (keV)	EABS(e^+) (keV)
Air	0.05	0.05	1.0	0.1	1.0	0.1	0.1
Al	0.1	0.1	10.0	1.0	10.0	1.0	1.0
Cu	0.2	0.2	10.0	1.0	100.0	10.0	10.0
Steel	0.01	0.01	1.0	0.1	1.0	0.1	0.1
W (collimators)	0.15	0.15	10.0	1.0	10.0	1.0	1.0
W (target)	0.01	0.01	1.0	0.1	1.0	0.1	0.1
Water	0.02	0.02	1.0	0.1	1.0	0.1	0.1

For SRS treatments, the linac incorporates a DMLC whose detailed description can be found in González *et al* (2011). The DMLC is couples to the linac at 624 mm from the source and consists of 24 pairs of of independent leafs made of W, with a width of 1.9 mm. At the isocenter, the maximum radiation field that the DMLC may produce is of 7.0 cm×7.0 cm. Leaf junction is of tongue/groove type and in order to reduce the friction due to displacement, adjacent leafs are separated by 0.05 mm of air. Transmission through the DMLC is reduced because the leafs are slightly divergent. In their movement the leafs describe a convex path allowing the photon beam to be focused not only in the motion direction but also in the transverse one. The divergence in the leaf positioning was not included in the simulation geometry. All other features of the DMLC (leaf coupling, air space between leafs, material, etc.) have been modeled exactly as reported by the manufacturer.

The simulation was carried out in three steps. First a phase space file PSF-1 was scored at the exit of the head, with a total of $3 \cdot 10^{10}$ initial electrons. Then PSF-1 (with splitting factor of 10) was used to simulate the transmission through the DMLC. A second phase space file PSF-2 was obtained after it. Finally, PSF-2 was used to perform the simulations of dose profiles in water.

To reduce the CPU time two simplifications were assumed. First, only those

electrons present in PSF-1 and hitting the DMLC in the air space between leafs were followed in the simulations. The electrons impinging directly on the leafs were expected to be absorbed in the DMLC and were not simulated. In addition, only Compton interactions have been considered for photons transported through the DMLC.

In González *et al* (2011) the values of the simulation parameters and material densities used, as well as the approximations made in the DMLC geometry model and transmission, were validated against dose profile measurements. In general, a good agreement was found between the simulated profiles and those measured with a PTW Diode 60008 and a PTW Semiflex 31010 chamber (PTW, Freiburg, Germany). One of the results obtained therein was the necessity of reducing the separation between the DMLC leafs from 0.05 mm, the value quoted by the manufacturer, to 0.0197 mm in order to reproduce the experimental data. On the other hand, considering in the DMLC only Compton interactions does not modify significantly the results obtained in a complete simulation of the photon transport throughout the DMLC and reduces the CPU time by a factor 50.

References

Alfonso R, Andreo P, Capote R, Huq M S, Kilby W, Kjäll P, Mackie T R, Palmans H, Rosser K, Seuntjens J, Ullrich W and Vatnitsky S 2008 A new formalism for reference dosimetry of small and nonstandard fields *Med. Phys.* **35** 5179-86

Chetty I J, Curran B, Cygler J E, DeMarco J J, Ezzell G, Faddegon B A, Kawrakow I, Keall P J, Liu H, Ma CM, Rogers D W, Seuntjens J and Sheikh-Bagheri D 2007 Report of the AAPM Task Group No. 105: Issues associated with clinical implementation of Monte Carlo-based photon and electron external beam treatment planning. *Med. Phys.* **34** 4818-53

Das I J, Ding G X and Ahnesjö A 2008 Small fields: Nonequilibrium radiation dosimetry. *Med. Phys.* **35** 206-15

Fippel M, Haryanto F, Dohm, Dohm O, Nüsslin F and Kriesen S 2003 A virtual photon energy fluence model for Monte Carlo dose calculation. *Med. Phys.* **30** 301-11

Fix M K, Cygler J, Frei D, Volken W, Neuenschwander H, Born E J and Manser P 2013 Generalized eMC implementation for Monte Carlo dose calculation of electron beams from different machine types *Phys. Med. Biol.* **58** 2841-59

González W, Anguiano M and Lallena A M 2015a A source model for the electron contamination of clinical linac heads in photon mode *Biomed. Phys. Eng. Express* **1** 025202

González W, García-Ferreira I-B, Anguiano M and Lallena A M 2015b A general photon source model for clinical linac heads in photon mode *Radiat. Phys. Chem.* **117** 140-52

González W, Lallena A M and Alfonso R 2011 Monte Carlo simulation of the dynamic micro-multileaf collimator of a LINAC Elekta Precise using PENELOPE. *Phys. Med. Biol.* **56** 3417-31

International Atomic Energy Agency 2004 *Commissioning and quality assurance of computerized planning systems for radiation treatment of cancer* IAEA Technical Report Series 430 (Vienna: IAEA)

Paskalev K, Seuntjens J, Patrocinio H and Podgorsak E B 2003 Physical aspects of dynamic stereotactic radiosurgery with very small photon beams *Med. Phys.* **30** 111-8

Press W H, Teukolsky S A, Vetterling W T and Flannery B P 1992 *Numerical recipes in Fortran* 2nd edn (New York: Cambridge University Press)

Salvat F, Fernández-Varea J M, Sempau J 2014 *PENELOPE - A code system for Monte Carlo simulation of electron and photon transport* (Barcelona: NEA)

Scott A J D, Nahum A E and Fenwick J D 2008 Using a Monte Carlo model to predict dosimetric properties of small radiotherapy photon fields *Med. Phys.* **35** 4671-84

Sempau J, Wilderman S J and Bielajew A F 2000 DPM, a fast, accurate Monte Carlo code optimized for photon and electron radiotherapy treatment planning

dose calculations *Phys. Med. Biol.* **45** 2263-91

Sham E, Seuntjens J, Devic S and Podgorsak E B 2008 Influence of focal spot on characteristics of very small diameter radiosurgical beams *Med. Phys.* **35** 3317-30

Sikora M and Alber M 2009 A virtual source model of electron contamination of a therapeutic photon beam *Phys. Med. Biol.* **54** 7329-44

Sikora M, Dohm O and Alber M 2007 A virtual photon source model of an Elekta linear accelerator with integrated mini MLC for Monte Carlo based IMRT dose calculation *Phys. Med. Biol.* **52** 4449-63

Traneus E, Ahnesjö A and Åsell A 2001 Application and verification of a coupled multi-source electron beam source model for Monte Carlo based treatment planning *Radiother. Oncol.***61** S102

Vandervoort E J, Tchistiakova E, La Russa D J and Cygler J E 2014 Evaluation of a new commercial Monte Carlo dose calculation algorithm for electron beams. *Med. Phys.* **41** 021711

Yang J, Li J. S, Qin L, Xiong W and Ma C-M 2004 Modeling of electron contamination in clinical photon beams for Monte Carlo dose calculation. *Phys. Med. Biol.* **49** 2657-73